This is the accepted manuscript made available via CHORUS. The article has been published as:

# Microscopic observation of hidden Johari-Goldstein-β process in glycerol

Makina Saito, Masayuki Kurokuzu, Yoshitaka Yoda, and Makoto Seto

Phys. Rev. E **105**, L012605 — Published 27 January 2022

DOI: 10.1103/PhysRevE.105.L012605

# Microscopic observation of hidden Johari-Goldstein-β process in glycerol

Makina Saito[1,2]*, Masayuki Kurokuzu[1], Yoshitaka Yoda[3], Makoto Seto[1]

[1] *Institute for Integrated Radiation and Nuclear Science, Kyoto University, Kumatori, Osaka 590-0494, Japan*

[2] *Department of Physics, Tohoku University, Sendai, Miyagi 980-8578, Japan.*

[3] *Japan Synchrotron Radiation Research Institute, Sayo, Hyogo 679-5198, Japan*

E-mail: makina.saito.d6@tohoku.ac.jp

## Abstract

The Johari-Goldstein-(JG)-β process is widely observed in a variety of glass-forming systems and recognized as an intrinsic process in deeply supercooled and glassy states. However, in some systems e.g. glycerol, a clear sign of the JG-β process is often not apparent; for example, an isolated JG-β peak may not be observed in the dielectric relaxation spectrum. In this study, we directly investigated the angstrom-scale dynamics of glycerol through quasi-elastic scattering experiments using time-domain interferometry. The relaxation times of the local motions start to decouple from the time scale of the diffusion process and follow the established behavior of the JG-β process. This finding microscopically indicates the existence of the hidden JG-β process in glycerol. In addition, we succeeded in determining the decoupling temperature of the JG-β process by using the spatial-scale selectivity of the quasi-elastic scattering technique.

In the 1970s, Johari and Goldstein systematically studied the dynamics of many glass-forming systems using dielectric relaxation spectroscopy, often observing an isolated peak in addition to the main peak related to the diffusion (α) process [1–3]. Nowadays, this additional process is called the Johari–Goldstein (JG) β process, recognized as an intrinsic process in deeply supercooled and glass states [4,5]. In the relaxation spectrum of a deeply supercooled system, the JG-β process starts to appear on the high-frequency (shorter time scale) side of the α process peak, branching from the α process with cooling [1–5]. The coupling model has been successfully employed to explain the relation between the JG-β process and the α process, proposing that the JG-β process acts as a precursor for the α process in supercooled states [5]. At $T_g$, the α-relaxation time reaches 100 s, while the time scale of the JG-β process is much shorter, around microseconds and milliseconds, owing to the relatively moderate temperature dependence of the JG-β process [1–5]. As for a picture of how the relaxation occurs in real space, some experiments such as NMR have revealed that the JG-β process is spatially restricted and occurs more uniformly and locally compared with the α process [5–11]. However, Johari ascribed the origin to the rotational and/or translational motion of a small subset of molecules with distinct dynamical behavior, the movement of which cannot be trivially associated with a uniform response [4,12]. Because the microscopic dynamics associated with the JG-β relaxation have not yet been fully observed, a microscopic picture of the JG-β process remains controversial.

The JG-β process is widely observed in a variety of systems, such as structural glass-formers, orientational glasses, and biosystems, and is known to control some of their macroscopic properties [1–5]. However, the JG-β process is not clearly observed in some glass-forming systems using any method, including dielectric relaxation spectroscopy (DRS), which is one of the most powerful tools for investigating the JG-β process because of its broadband characteristics [7,13,14]. In some glass-forming systems, an excess tail of the α peak, denoted as the excess wing (EW), is observed on the high-frequency side of the α peak in the dielectric relaxation spectra, instead of a clear JG-β peak [7,15–17]. Glycerol is one of the most famous examples of such materials [7,15–22]. Several origins have been proposed for the EW of glycerol: the JG-β process [18–20], a process other than the JG-β process [21], and both the excess high-frequency component of the α process and the JG-β process [22]. This controversy regarding the common existence of the JG-β process and the origin of EW hinders the establishment of a general dynamical view of glass-forming systems.

Herein, we report clear evidence for the presence of the JG-β process in glycerol, as microscopically revealed via quasi-elastic gamma-ray scattering (QEGS) using multi-line

time-domain interferometer (TDI) [23–25]. Quasi-elastic scattering techniques allow for the determination of microscopic relaxation times with the specification of the spatial scale by selecting the momentum transfer $q$ [26–29]. It has been established that the local JG-β process can be observed via QEGS using TDI in the large $q$ region corresponding to the local spatial scale (such as a few angstroms) distinctly from the α process observed in the smaller $q$ region [10,26–29]. Owing to this selectivity, we succeeded in clearly observing the JG-β process and determined the decoupling temperature of the JG-β process in glycerol.

Anhydrous glycerol (>99.5%) purchased from Sigma-Aldrich (St. Louis, MO, USA) was treated in a $N_2$ atmosphere to avoid contact with humid air. TDI-QEGS experiments were performed at the nuclear resonant scattering beamline of SPring-8 (Japan) in an operating mode with a bunch interval of 684.3 ns. Directional Mössbauer gamma rays (with energy of 14.4 keV and energy width of ~4.7 neV) from $^{57}$Fe nuclei were utilized for the QEGS measurements using multi-line TDI [24,25]. As shown in Fig. 1(A), QEGS using multi-line TDI covers the typical time and spatial scales dominated by the JG-β process [24,25]. Therefore, this technique is ideal for microscopically observing the JG-β process. The diffraction pattern of glycerol is shown in Fig. 1(B). A Si-Avalanche photodiode detector was used to detect scattering photons. The detector was placed at angles corresponding to $q$ = 15, 41, and 58 nm$^{-1}$. The three $q$ regions covered by the detectors are shown in Fig. 1(B). The measurements were performed at temperatures of 185, 195, 205, 215, 220, 225, 230, 235, 240, 245, 250, 255, and 260 K, including $T_g$ = 185 K.

In Fig. 2 (A), the time spectra obtained at 185, 220, 230, 240, and 250 K at $q$ = 15 nm$^{-1}$ are shown. The QEGS spectra $\overline{I_{\mathrm{QEGS}}}(q,t)$ can be expressed as:

$$\overline{I_{\mathrm{QEGS}}}(q,t) \propto \{1 - I^{e\prime}(q,t)\}\{I_1(t) + I_2(t)\} + I^{e\prime}(q,t)I_{1+2_{\mathrm{coh}}}(t) - \{1 - f_{\Delta E}(q)\}I_2(t), \quad (1)$$

where $I^{e\prime}(q,t)$ is the experimentally obtained ISF normalized by the value at time $t$ = 0; $f_{\Delta E}$ is a fitting parameter containing information of dynamics in the picosecond time scale; $t$ is the time [25]; $I_1(t)$, $I_2(t)$, and $I_{1+2_{\mathrm{coh}}}(t)$ are the reference time spectra of gamma rays from the upstream, downstream, and gamma-ray emitters, respectively [25]. The Kohlrausch–Williams–Watts (KWW) function $f_{\Gamma 0}\exp\{-(t/\tau)^{\beta_{\mathrm{KWW}}}\}$ is assumed to be the relaxation function of $I^{e\prime}(q,t)$ of each QEGS spectrum, where $f_{\Gamma 0}$, $\tau$, and $\beta_{\mathrm{KWW}}$ are the intensity of the relaxation, relaxation time, and stretching parameter, respectively.

A DRS study reported that $\beta_{\mathrm{KWW}}$ of the α process apparently decreases with cooling [17]. Therefore, the temperature dependence of $\beta_{\mathrm{KWW}}$ was considered for fitting the obtained time spectra to precisely determine the relaxation times. The DRS result

validates the linear temperature ($T$) dependence of $\beta_{\mathrm{KWW}}$ as $\beta_{\mathrm{KWW}}(T) = a + bT$, where $a$ and $b$ are constants [17]. We performed global fitting for all time spectra at the diffraction peak ($q$ = 15 nm$^{-1}$) using the linear temperature dependence with free $a$ and $b$ parameters and other respective free parameters such as $f_{\Gamma 0}$ and $\tau$ for each spectrum. The fitting curves of the time spectra are shown in Fig. 2(A): the time spectra are well fitted. We determined $a$ = 0.43 (±0.08) and $b$ = 1.4×10$^{-3}$ (±0.2×10$^{-3}$) K$^{-1}$. At 220 K, for example, the $\beta_{\mathrm{KWW}}$ value for $q$ = 15 nm$^{-1}$ is 0.7. This $\beta_{\mathrm{KWW}}$ value is consistent with that of the α process obtained via DRS [17]. In Fig. 2(B), the evaluated ISF from the experimental time spectra are presented, confirming that the evaluated ISF is explained by the KWW function (solid curves) determined by the fitting.

The mean relaxation time $\langle\tau\rangle$ was calculated for each temperature and $q$ point as $\langle\tau\rangle = \tau\Gamma(1/\beta_{\mathrm{KWW}})/\beta_{\mathrm{KWW}}$, where Γ is the gamma function. The obtained temperature dependence of $\langle\tau\rangle$ at $q$ = 15 nm$^{-1}$ is shown in Fig. 3(A) as filled circles in a so-called Angell plot. At $q$ = 15 nm$^{-1}$, the temperature dependence is sufficiently explained by the Vogel–Fulcher–Tammann (VFT) law (solid curve). To reveal the microscopic origin of the relaxations observed at $q$ = 15 nm$^{-1}$, we compared the obtained relaxation time with the DRS relaxation times. The α-relaxation time $\tau_\alpha$ obtained via DRS is displayed in Fig. 3(B) as a black solid curve together with the relaxation times obtained by the present study at $q$ = 15 nm$^{-1}$ (filled circles) [17]. Though these relaxation times should be carefully compared due to the difference of the origin of the relaxations probed by these methods, as discussed in Ref. 30, the order of the time scale of the relaxations can be comparable. The α-relaxation time of DRS exhibits a similar time scale to the relaxation time obtained by the present study at the diffraction peak. This agreement confirms that the α process mainly dominates the structural relaxation motions observed at the diffraction peak ($q$ = 15 nm$^{-1}$) [26,27].

For time spectra obtained at $q$ = 41 and 58 nm$^{-1}$, we performed a similar analysis with a fixed $b$ = 1.4×10$^{-3}$ value obtained through the analysis for $q$ = 15 nm$^{-1}$ due to relatively low statistics. The time spectra are well fitted and the $a$ value was determined by the global fitting as 0.18 (±0.07). At 220 K, the $\beta_{\mathrm{KWW}}$ values for $q$ = 41 and 58 nm$^{-1}$ were approximately 0.5, which was found to be lower than the value at $q$ = 15 nm$^{-1}$. In Figs. 2(C,D), we present the evaluated ISF from the experimental time spectra for $q$ = 41 and 58 nm$^{-1}$, respectively.

The obtained temperature dependences of $\langle\tau\rangle$ at $q$ = 41 and 58 nm$^{-1}$ are respectively depicted as the filled triangles and diamonds in Figs. 3(A) and 3(B). At large $q$ regions, the change in the temperature dependence from the VFT to the Arrhenius law is commonly observed through cooling. In the low temperature region of 0.82 < $T_g/T$ < 1,

we fitted the temperature dependence by the Arrhenius law for $q$ = 41 and 58 nm$^{-1}$. The fitting curves are shown as the dashed lines.

Very similar relaxation behaviors have been reported in the large $q$ regions of *o*-terphenyl, polybutadiene, and 5-methyl-2-hexanol in comparable $T_g/T$ regions via QEGS using TDI [26–28]. The origin of the local-scale relaxations was found to be the JG-β process [26–28]. The quantitative similarity summarized in Table I is clear enough that the local-scale relaxation observed for glycerol can be attributed to the same origin. Namely, the JG-β process commonly dominates local-scale relaxations observed in the $q$ region above several tens of nm$^{-1}$, as shown in Table I. The temperature at which the local-scale motions start to follow the Arrhenius law by cooling is treated as the branching temperature of the JG-β process $T_{\alpha\beta}$ [26,27]. We could determine $T_{\alpha\beta}$ as $T_g/T_{\alpha\beta} \sim 0.82$, which is close to the $T_g/T_{\alpha\beta}$ values of other glass-forming systems reported thus far via QEGS [26–28]. The evaluated activation energies $E$ were 28 (±8) and 26 (±4) kJ/mol obtained for $q$ = 41 and 58 nm$^{-1}$, respectively, which are comparable to those obtained at similar $q$ scales (several tens of nm$^{-1}$) for other glass-forming systems observed via QEGS using TDI, as shown in Table I, and reasonable for the JG-β process [22].

In a previous study, dielectric relaxation spectra were analyzed by assuming a single peak for EW [17]. The obtained time scale $\tau_{EW}$, shown as empty circles in Fig. 3(B), is the representative time scale for EW [17]. The temperature dependence of $\tau_{EW}$ is similar to that of the α-relaxation time. Therefore, the origin of the major part of the EW is interpreted to be the excess high-frequency component of the α process. In contrast, the temperature dependence of the JG-β relaxation time obtained in the present study is apparently different from the temperature dependences of the α-relaxation time and $\tau_{EW}$. Here, in the dielectric relaxation spectra, the EW of glycerol spreads over very wide frequency (time) scales and the broad EW time ranges fully include the time scale of the JG-β process determined in the present study [17]. This result suggests that both the excess high-frequency component of the α process and the relatively week JG-β peak contribute to the EW. Thus, analysis of the EW region in the dielectric relaxation spectra requires a quantitative line-shape analysis assuming both contributions. Through careful observation of the aging phenomenon in glycerol, both contributions to the EW region have been revealed so far [18,22]. Based on this observation, a line-shape analysis of the DRS results was previously performed by assuming a relatively weak peak for the JG-β process and the power-law tail, which expresses the excess high-frequency contribution of the α process [22]. The time scale of the JG-β process $\tau_{JG\beta}$ obtained from the line-shape analysis is indicated by the empty triangles in Fig. 3(B) [22]. The temperature-dependence behavior of $\tau_{JG\beta}$ agrees well with that of the JG-β relaxation times obtained

in the present study. This agreement strongly supports our result that the JG-β process contributes to EW in addition to the excess high-frequency component of the α process.

In Fig. 3(B), the time scales of the translational collective dynamics obtained through neutron spin echo (NSE) at very low $q$ = 0.74 nm$^{-1}$ are plotted as cross points [30]. The spatial scale of the observed corrective motions is $2\pi/q$ ~ 8.5 nm. The collective nanometric-scale relaxation times are close to the α-relaxation time of DRS in the high-temperature region ($T_g/T$ < 0.8) [30]. We found that the relaxations at $q$ = 15 nm$^{-1}$ (4-Å scale) are dominated by the α process in the present study. Therefore, the α process dominates the dynamics on a collective spatial scale larger than several angstroms, while the local-scale relaxations observed at $q$ = 41 and 58 nm$^{-1}$ (1-Å scale) are mainly caused by the JG-β process. At $T_g/T$ = 0.87, the collective relation time determined via NSE deviates from the α-relaxation time as shown in Fig. 3(B) [30]. The observed relaxation is too fast to be ascribed to the JG-β process. Such an interpretation is also inconsistent with the locally restricted relaxation picture of the JG-β process revealed so far [5–11]. The data at $T_g/T$ = 0.87 is close to $\tau_{EW}$, whose major origin was ascribed to the excess high-frequency component of the α process in the above discussion. Therefore, we assume that the excess high-frequency component of the α process is observed at $T_g/T$ = 0.87 instead of the major part of the α process, whose relaxation time $\tau_\alpha$ is too long to be detected at this temperature. To elucidate a more detailed microscopic picture to explain the excess high-frequency component, further dynamic measurements are required in the relatively low $q$ region.

In this study, we demonstrated the existence of a local-scale JG-β process in glycerol from a microscopic viewpoint. We microscopically revealed that both the JG-β process and the excess high-frequency component of the α process contribute to EW in the dielectric relaxation spectra. The spatial-scale selectivity of QEGS allows for selective observation of the JG-β process at relatively high $q$ even near the decoupling temperature of the JG-β process from the α process. This enabled us to determine the branching temperature of the JG-β process from the α process as $T_g/T_{\alpha\beta}$ ~ 0.82. The dynamic information uncovered in this work and the thermodynamics of such systems can be integrated into an energy landscape view, whose understanding is key to revealing the time-space evolution of the JG-β process e.g. its relationship to the α process above $T_g$ and the microscopic mechanism behind aging phenomena below $T_g$ [4,5,31]. The local structure of the energy landscape can be further investigated by combining QEGS and calorimetry studies [32,33].

## References


1. G. P. Johari and M. Goldstein, J. Phys. Chem. **74**, 2034 (1970).
2. G. P. Johari and M. Goldstein, J. Chem. Phys. **53**, 2327 (1970).
3. G. P. Johari and M. Goldstein, J. Chem. Phys. **55**, 4245 (1971).
4. G. P. Johari J. Phys. Chem. B **123**, 3010 (2019).
5. K. L. Ngai, *Relaxation and diffusion in complex systems* (Springer, Berlin, 2011).
6. H. Wagner and R. Richert, J. Non-Cryst. Solids **242**, 19 (1998).
7. A. Kudlik, S. Benkhof, T. Blochowicz, C. Tschirwitz, and E. Rössler, J. Mol. Struct. **479**, 210 (1999).
8. M. Vogel and E. A. Rössler, J. Phys. Chem. **104**, 4285 (2000).
9. M. Vogel, P. Medick, and E. A. Rössler, Ann. Rep. NMR Spectr. **56**, 231 (2005).
10. D. Richter, R. Zorn, B. Farago, B. Frick, and L. J. Fetters, Phys. Rev. Lett. **68**, 71 (1992).
11. G. Williams and D. C. Watts, Trans. Faraday Soc. **67,** 1971 (1971).
12. G.P. Johari, J. de Chimie **82,** 283 (1985).
13. F. Kremer, A. Schönhals (Eds.), *Broadband Dielectric Spectroscopy* (Springer, Berlin, 2002).
14. P. Lunkenheimer, U. Schneider, R. Brand, and A. Loidl, Contemp. Phys. **41**, 15 (2000).
15. P. K. Dixon, L. Wu, S. R. Nagel, B. D. Williams, and J. P. Carini, Phys. Rev. Lett. **65**, 1108 (1990).
16. P. Lunkenheimer, A. Pimenov, B. Schiener, R. Böhmer, and A. Loidl, Europhys. Lett. **33**, 611 (1996).
17. P. Lunkenheimer and A. Loidl, Chem. Phys. **284**, 205 (2002).
18. U. Schneider, R. Brand, P. Lunkenheimer, and A. Loidl, Phys. Rev. Lett. **84**, 5560 (2000).
19. T. Blochowicz and E. A. Rössler, Phys. Rev. Lett. **92**, 225701 (2004).
20. A. A. Pronin, M. V. Kondrin, A. G. Lyapin, V. V. Brazhkin, A. A. Volkov, P. Lunkenheimer, and A. Loidl, Phys. Rev. E **81**, 041503 (2010).
21. S. Hensel-Bielowka and M. Paluch, Phys. Rev. Lett. **89**, 025704 (2002).
22. C. Gainaru, R. Kahlau, E. A. Rössler, and R. Böhmer, J. Chem. Phys. **131**, 184510 (2009).
23. A. Q. R. Baron, H. Franz, A. Meyer, R. Rüffer, A. I. Chumakov, E. Burkel, and W. Petry, Phys. Rev. Lett. **79**, 2823 (1997).

24. M. Saito, M. Seto, S. Kitao, Y. Kobayashi, M. Kurokuzu, and Y. Yoda, Hyperfine Interact. **206**, 87 (2012).
25. M. Saito, R. Masuda, Y. Yoda, and M. Seto, Sci. Rep. **7**, 12558 (2017).
26. M. Saito, S. Kitao, Y. Kobayashi, M. Kurokuzu, Y. Yoda, and M. Seto, Phys. Rev. Lett. **109**, 115705 (2012).
27. T. Kanaya, R. Inoue, M. Saito, M. Seto, and Y. Yoda, J. Chem. Phys. **140**, 144906 (2014).
28. F. Caporaletti, S. Capaccioli, S. Valenti, M. Mikolasek, A. I. Chumakov, and G. Monaco, Sci. Rep. **9**, 14319 (2019).
29. F. Caporaletti, S. Capaccioli, S. Valenti, M. Mikolasek, A. I. Chumakov, and G. Monaco, Nat. Commun. **12**, 1867 (2021).
30. S. Gupta, N. Arend, P. Lunkenheimer, A. Loidl, L. Stingaciu, N. Jalarvo, E. Mamontov, and M. Ohl, Eur. Phys. J. E **38**, 1 (2015).
31. E. Tombari and G. P. Johari J. Phys. Chem. B **124**, 2017 (2020).
32. M. Goldstein, J. Chem. Phys. **51**, 3728 (1969).
33. C. A. Angell, J. Non-Cryst. Solids **131**, 13 (1991).

**Acknowledgments:**

We are grateful for Prof. Y. Wakabayashi (Tohoku University) for his valuable comments. This work was supported by JSPS KAKENHI (Grant-in-Aid for Young Scientists) Grant Number 19K20600, and JST CREST Grant Number JPMJCR2095, Japan. The investigation was performed with the approval of the Japan Synchrotron Radiation Research Institute (Proposal Nos. 2018A1137, 2018B1161, 2019B1299, and 2021A2087).

**Figure 1.**

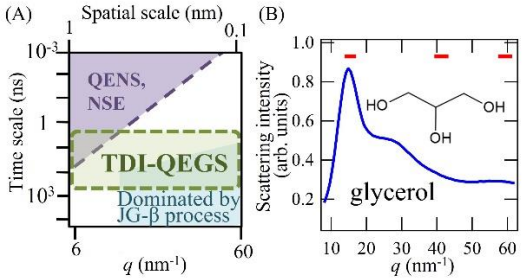



FIG. 1. Spatial and time scales of dynamics covered by some quasi-elastic gamma-ray scattering techniques and diffraction pattern of glycerol.
(A) Spatial (momentum transfer $q$) scale and time scale of dynamics covered by TDI-based quasi-elastic gamma-ray scattering techniques (TDI-QEGS), quasi-elastic neutron scattering (QENS), and neutron spin echo (NSE). (B) Diffraction profile of glycerol. The $q$ regions covered by the detectors are indicated by the bars.

**Figure 2.**

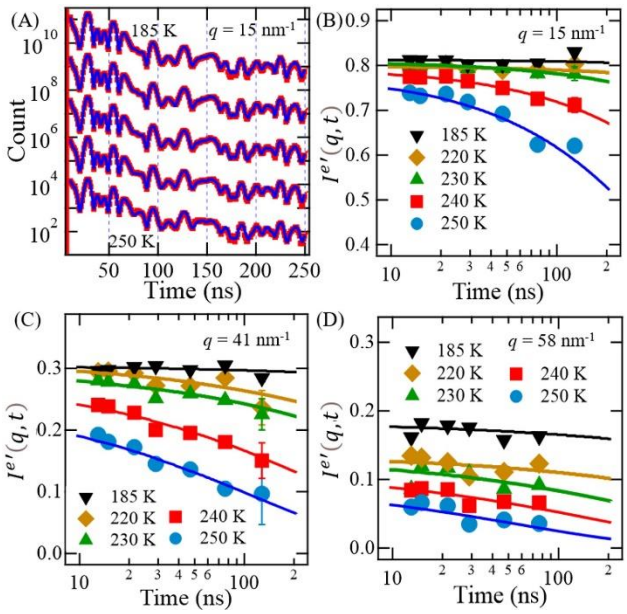



FIG. 2. Time spectra and intermediate scattering functions.
(A) Time spectra (red points) obtained at 185, 220, 230, 240, and 250 K at $q$ = 15 nm$^{-1}$. Solid lines indicate the fitting curves. (B) Normalized intermediate scattering function $I^{e\prime}(q,t)$ evaluated by the fitting for each temperature at $q$ = 15 nm$^{-1}$. Solid curves are the Kohlrausch–Williams–Watts function determined by fitting. $I^{e\prime}(q,t)$ obtained at (C) $q$ = 41 nm$^{-1}$, and (D) $q$ = 58 nm$^{-1}$.

**Figure 3.**

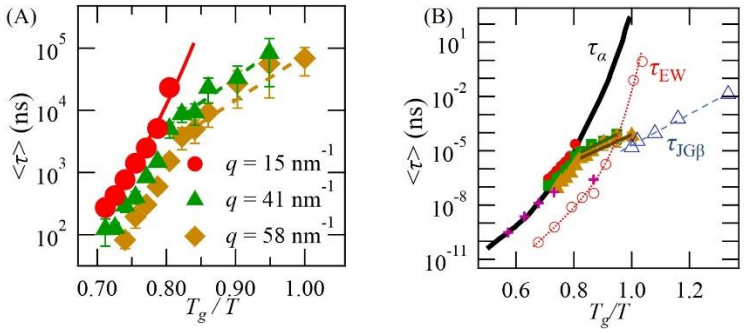



FIG. 3. Temperature dependence of the relaxation time.
(A) Temperature dependence of the mean relaxation time obtained at $q$ = 15, 41, and 58 nm$^{-1}$. Red curve indicates the VFT fit for the mean relaxation time obtained at $q$ = 15 nm$^{-1}$. Dashed lines are the fitting curves by the Arrhenius law for the mean relaxation time obtained at $q$ = 41 and 58 nm$^{-1}$. (B) Temperature dependence of the mean relaxation time determined from various methods. The symbols of the mean relaxation times obtained in the present study are the same as those in (A). Solid line is the α-relaxation time realized via DRS [16]. The time scales of EW $\tau_{EW}$ determined by assuming a single peak for EW in the dielectric relaxation spectra are shown as empty circles [16]. Empty triangles are the JG-β relaxation time obtained from the line-shape analysis of the EW region of the dielectric relaxation spectra [21]. Dotted line and Dashed lines are guides for the eyes. Cross points are the collective relaxation time determined via NSE at $q$ = 0.74 nm$^{-1}$ [29].

TABLE I. Summary of $q$ range, branching temperature $T_g/T_{\alpha\beta}$, and activation energy $E$ of the JG-β process obtained via quasi-elastic scattering using TDI.

| | $q$ range ($nm^{-1}$) | $T_g/T_{\alpha\beta}$ | $E$ (kJ/mol) |
|---|---|---|---|
| *o*-terphenyl | 18, 23, 29 [25,26] | 0.86 [25,26] | 36 [25] |
| polybutadiene | 21, 27, 32, 39 [26] | 0.81 [26] | 20 [26] |
| 5-methyl-2-hexanol | 13, 24, 37 [27] | 0.83 [27] | 27 [27] |
| glycerol | 41, 58 | 0.82 | 26, 28 |